An Inner-Constrained Separation Technique for 3D Finite Element Modeling of GO Silicon Steel Laminations

Weiying Zheng[1], *Member, IEEE* and Zhiguang Cheng[2], *Senior Member, IEEE*

[1]LSEC, Academy of Mathematics and Systems Science, Chinese Academy of Sciences, Beijing, 100190, CHINA
[2]R & D Center, Baoding Tianwei Group Co., LTD, Baoding 071056, CHINA

Grain-oriented (GO) silicon steel laminations are widely used in iron cores and shielding structures of power equipments. When the leakage magnetic flux is very strong and enters the lamination plane perpendicularly, the eddy current loss induced there must be taken into account in electromagnetic design. It is preferable to accurately compute three-dimensional (3D) eddy currents at least in a few outer sheets of the lamination stack. Since the coating film applied to each sheet is only 2-5μm thick, finite element modeling of 3D eddy currents is very difficult in GO silicon steel laminations of large electromagnetic devices. This paper proposes an inner-constrained separation technique (ICST) to compute the 3D eddy currents. Instead of the coating film, the ICST introduces an inner constraint into the A-formulation to separate the laminations from each other. By the ICST, the 3D eddy currents can be computed accurately without meshing the coating film. Numerical experiments are carried out on the TEAM (Testing Electromagnetic Analysis Methods) benchmark model P21^c–M1 and the numerical results show good agreements with the measured data.

***Index Terms*—Eddy currents, finite element methods, GO silicon steel lamination, inner-constrained separation technique.**

I. Introduction

GRAIN-ORIENTED (GO) silicon steel laminations are widely used in iron cores and shielding structures of power equipments. The lamination stack usually consists of many steel sheets (0.18-0.35mm thick) and very thin coating films (2-5μm thick). Thus the lamination stack has multi-scale sizes and the ratio of the largest scale to the smallest scale can amount to 10^6. Full 3D finite element modeling is extremely difficult due to large numbers of elements from meshing both laminations and coating films.

In recent years, numerical methods have been widely studied for nonlinear eddy current problems in steel laminations. Among them, most works pay attention to effective reluctivities and conductivities of the lamination stack (cf. e.g. [1]–[5]). The main idea is to replace physical parameters with equivalent (or homogenized) parameters for Maxwell's equations. In [6]–[7], Bottauscio et al propose a mathematical homogenization technique based on the multiple scale expansion theory to derive the equivalent electric parameters and effective magnetization properties. In [8]–[9], Gyselinck et al deduce the effective material parameters by an orthogonal decomposition of the flux in the perpendicular and parallel directions to the lamination plane. In [10], Napieralska-Juszczak et al establish equivalent characteristics of magnetic joints of transformer cores by minimizing the magnetic energy of the system. Numerical methods based on the homogenization of material parameters provide an efficient way to simulate electromagnetic field in steel laminations. Since the effective conductivity is anisotropic and has zero value in the normal direction to the lamination plane, the numerical eddy current is thus two-dimensional in the lamination stack.

When the leakage magnetic flux is very strong and enters the lamination plane perpendicularly, for example, in the outer laminations of large power transformer core, the eddy current loss induced there must be taken into account in electromagnetic design. It is preferable to accurately compute 3D eddy currents at least in a few outer sheets of the lamination stack, that is, to use the zoned treatment for practical approaches, see Fig. 1. In such an accurate finite element analysis, one usually has to mesh both the laminations and the coating films in the 3D eddy current region. In [11], Cheng et al present an efficient macroscopic modeling method for iron cores. By meshing the laminations and the coating films in the 3D eddy current region, they investigated the effects of the eddy current, induced by the normal magnetic field, on the total iron loss and the distortion of the local magnetic flux in the laminations. More recently, some scientists paid attention to the study of the loss spectrum and electromagnetic behavior of laminated steel sheets in the literature (cf. e.g. [12]–[17]).

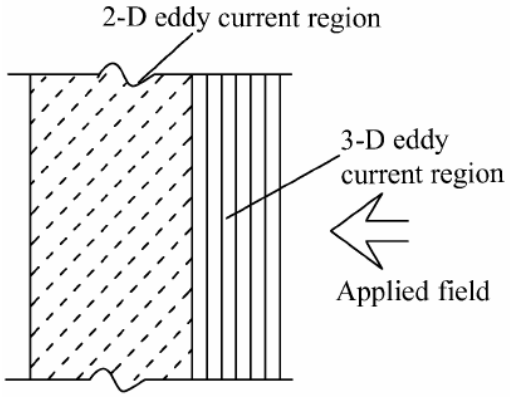

Fig. 1 Zoned treatment of the lamination stack.
The six laminations close to the source have isotropic conductivity and are meshed individually.

The main objective of this paper is to propose an inner-constrained separation technique (ICST) for the finite element computation of 3D eddy currents in silicon steel laminations. The eddy current is confined in each lamination by the coating film. The treatment of this property plays the key role in

Manuscript received October 9, 2011. Corresponding author: Weiying Zheng (e-mail: zwy@lsec.cc.ac.cn).
Digital Object Identifier inserted by IEEE

designing efficient numerical methods for computing 3D eddy currents. The standard approach is to mesh the coating film and set the conductivity by zero there (see [11]). It usually leads to very anisotropic meshes and large numbers of elements, and as a result, the discrete problem will be very difficult to solve. The ICST introduces an inner constraint on the magnetic vector potential to replace the coating film so that the eddy current is still conserved in each lamination. The main merit is that it need not partition the coating film in finite element modeling.

The finite element approximation of the nonlinear eddy current problem is solved by an inexact Newton method and an alternating iteration algorithm. We implement the ICST finite element method based on MPI (Message Passing Interface) and unstructured tetrahedral meshes. The proposed method and the parallel program are tested by the TEAM Benchmark Problem 21^c–M1. The numerical results show good agreements with the measurement data.

II. The **A**-formulation of eddy current problems

In the **A**-formulation of the eddy current model, $\mathbf{A}$ denotes the magnetic vector potential satisfying $\operatorname{curl}\mathbf{A}=\mathbf{B}$ and $\mathbf{B}$ be the magnetic flux density. Then the **A**-formulation of the eddy current model reads (cf. e.g. [18]):

$$\begin{aligned} \sigma\frac{\partial\mathbf{A}}{\partial t}+\operatorname{curl}\left(\nu\operatorname{curl}\mathbf{A}\right)&=\mathbf{J}_s \quad \text{in} \quad \Omega,\\ \mathbf{A}\times\mathbf{n}&=0 \quad \text{on} \quad \Gamma \end{aligned} \tag{1}$$

where σ is the electric conductivity, ν is the nonlinear and anisotropic reluctivity, and $\mathbf{J}_s$ stands for the exciting source satisfying $\operatorname{div}\mathbf{J}_s=0$. Let Ω be the truncated domain with boundary Γ and $\mathbf{n}$ be the unit outer normal of Γ. The weak formulation of (1) reads: Find $\mathbf{A}\in\mathbf{H}_0(\operatorname{curl},\Omega)$ such that

$$\begin{aligned} \int_\Omega\sigma\frac{\partial\mathbf{A}}{\partial t}\cdot\mathbf{v}+\int_\Omega\nu\operatorname{curl}\mathbf{A}\cdot\operatorname{curl}\mathbf{v}&=\int_\Omega\mathbf{J}_s\cdot\mathbf{v}\\ \forall\,\mathbf{v}\in\mathbf{H}_0(\operatorname{curl},\Omega),& \end{aligned} \tag{2}$$

where $\mathbf{v}$ is the test function and

$$\begin{aligned} \mathbf{H}(\operatorname{curl},\Omega)&=\left\{\mathbf{u}\in\mathbf{L}^2(\Omega):\ \operatorname{curl}\mathbf{u}\in\mathbf{L}^2(\Omega)\right\},\\ \mathbf{H}_0(\operatorname{curl},\Omega)&=\left\{\mathbf{u}\in\mathbf{H}(\operatorname{curl},\Omega):\ \mathbf{u}\times\mathbf{n}=\mathbf{0}\ \text{ on }\ \Gamma\right\}. \end{aligned}$$

Throughout this paper, we shall denote vector-valued quantities by boldface notation, such as $\mathbf{L}^2(\Omega)=(L^2(\Omega))^3$, where $L^2(\Omega)$ is the space of square-integrable functions. Furthermore, we also define

$$\begin{aligned} H^1(\Omega)&=\left\{u\in L^2(\Omega):\ \nabla u\in\mathbf{L}^2(\Omega)\right\},\\ H_0^1(\Omega)&=\left\{u\in H^1(\Omega):\ u=0\ \text{ on }\ \Gamma\right\}. \end{aligned}$$

First we study the conservation property of eddy currents in steel laminations. It will provide the inspiration for deriving a new **A**-formulation which replaces the coating film with the ICST. Let $\Omega_c\subset\Omega$ denote the conducting region which consists of M laminations, namely,

$$\Omega_c=\Omega_1\cup\cdots\cup\Omega_M.$$

Since the coating film has positive thickness, $\Omega_1,\cdots,\Omega_M$ are viewed as isolated conductors (see Fig. 2), that is,

$$\operatorname{distance}(\Omega_i,\Omega_j)>0 \quad \text{for } i\neq j. \tag{3}$$

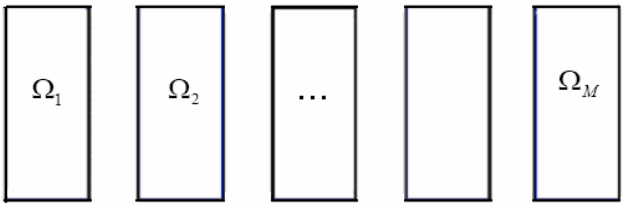

Fig. 2 A two-dimensional illustration of isolated conductors.

Let $\mathbf{J}=\sigma\dfrac{\partial\mathbf{A}}{\partial t}$ be the eddy current density. We state that the weak formulation (2) implies the conservation of $\mathbf{J}$ in each lamination. In fact, since $\nabla H_0^1(\Omega)\subset\mathbf{H}_0(\operatorname{curl},\Omega)$, taking $\mathbf{v}=\nabla\varphi$ in (2) yields

$$\int_\Omega\mathbf{J}\cdot\nabla\varphi=0 \qquad \forall\,\varphi\in H_0^1(\Omega), \tag{4}$$

which by (3) is equivalent to

$$\int_{\Omega_i}\mathbf{J}\cdot\nabla\varphi_i=0 \quad \forall\,\varphi_i\in H^1(\Omega_i),\ 1\le i\le M. \tag{5}$$

Then using integration by parts and the arbitrariness of φ_i, we obtain the conservation of $\mathbf{J}$ in each Ω_i:

$$\begin{cases} \operatorname{div}\mathbf{J}=0 & \text{in} \quad \Omega_i\\ \mathbf{J}\cdot\mathbf{n}=0 & \text{on} \quad \partial\Omega_i, \end{cases} \qquad 1\le i\le M. \tag{6}$$

The conditions in (6) indicate that the eddy currents, or the laminations, are separated by the coating film. Numerical methods for computing 3D eddy currents should satisfy these conditions. In the next section, we shall assume that the thickness of the coating film is zero and derive a new **A**-

formulation satisfying (6). The idea is to separate the laminations by an inner constraint instead of the coating film. It is thus named as the "Inner-Constrained Separation Technique".

III. A NEW **A**-FORMULATION BASED ON ICST

Now we suppose that the thickness of the coating film is zero (see Fig. 3). Then we have

$$\Omega_c = \bigcup_{i=1}^{M} \Omega_i, \qquad \text{distance}(\Omega_i, \Omega_{i+1}) = 0. \tag{7}$$

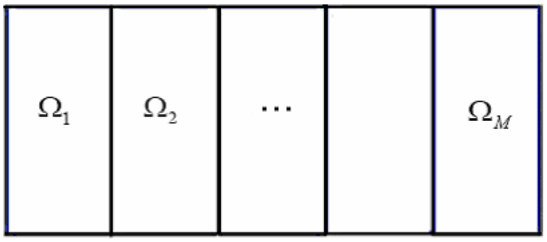

Fig. 3 Adjacent steel laminations without coating films.

Remember from (6) that the conservation of $\mathbf{J}$ is ensured by (5). Now for Ω_c satisfying (7), equation (5) is equivalent to

$$\begin{aligned} &\int_\Omega \mathbf{J}\cdot\nabla\varphi = 0 \quad \forall\, \varphi \in H_0^1(\Omega), \\ &\int_{\Omega_i} \mathbf{J}\cdot\nabla\varphi_i = 0 \quad \forall\, \varphi_i \in H^1(\Omega_i) \text{ and even } i. \end{aligned} \tag{8}$$

A comparison of (8) and (5) indicates that the test function space should contain the gradient of every $\varphi \in H^1(\Omega_i)$ for even index i. Thus the test function space in (2) is enlarged from $\mathbf{H}_0(\text{curl},\Omega)$ to $\mathbf{H}_0(\text{curl},\Omega)+\mathbf{U}$ where

$$\mathbf{U} = \left\{ \chi\cdot\nabla\varphi :\ \varphi \in H_0^1(\Omega) \right\}, \tag{9}$$

and χ is the characteristic function satisfying

$$\chi = \begin{cases} 1 & \text{in } \ \Omega_2 \cup \Omega_4 \cup \cdots, \\ 0 & \text{elsewhere.} \end{cases}$$

For Ω_c satisfying (7), we propose a new **A**-formulation as follows: Find $\mathbf{A} \in \mathbf{H}_0(\text{curl},\Omega)$ and $\mathbf{u} \in \mathbf{U}$ such that

$$\begin{aligned} &\int_\Omega \sigma \frac{\partial(\mathbf{A}+\mathbf{u})}{\partial t}\cdot(\mathbf{v}+\mathbf{w}) + \int_\Omega \nu\ \text{curl}\,\mathbf{A}\cdot\text{curl}\,\mathbf{v} \\ &\quad = \int_\Omega \mathbf{J}_s\cdot(\mathbf{v}+\mathbf{w}) \quad \forall \mathbf{v} \in \mathbf{H}_0(\text{curl},\Omega),\ \mathbf{w}\in\mathbf{U}, \end{aligned} \tag{10}$$

where $\mathbf{v}, \mathbf{w}$ are test functions and the magnetic reluctivity ν depends on the flux density $\mathbf{B} = \text{curl}\,\mathbf{A}$. In fact, $\mathbf{u}$ plays the role of an inner constraint on $\mathbf{A}$ so that the current density $\mathbf{J} = \sigma\dfrac{\partial}{\partial t}(\mathbf{A}+\mathbf{u})$ fulfils the conservation property in (6). The constraint function $\mathbf{u}$ can be solved by nodal element method only in Ω_i for even index i (see Fig. 4). The merit of (10) is that the coating films do not appear in the computational domain and the isotropic conductivity σ induces 3D eddy current in each lamination.

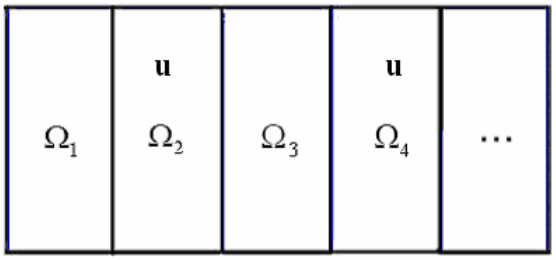

Fig. 4 The constraint function is only solved in $\Omega_2, \Omega_4, \cdots$.

To end this section, we remark that the solution of (10) is not unique. If $(\mathbf{A},\mathbf{u})$ solves (10), then $(\mathbf{A}-\nabla\xi, \mathbf{u}+\nabla\xi)$ also solves (10) for any smooth function ξ only supported in $\Omega_2 \cup \Omega_4 \cup \cdots$. However the magnetic flux density $\mathbf{B}$ and the eddy current density $\mathbf{J}$ are unique in the whole domain. Therefore it suffices to solve for one solution of (10) using some iterative methods.

IV. FINITE ELEMENT APPROXIMATION

In this section, we study the finite element approximation to (10) and propose an inexact Newton method for solving the nonlinear discrete problem. First we divide the time interval $[0, t_{end}]$ into small ones

$$0 = t_0 < t_1 < \cdots < t_M = t_{end},$$

and let $\tau_n = t_n - t_{n-1}$ be the time step size at t_n. Let $\mathfrak{I}_h$ be a tetrahedral mesh of Ω and define the nodal element space and the edge element space on $\mathfrak{I}_h$ by

$$\begin{aligned} \mathrm{Y}_h &= \left\{ v \in H_0^1(\Omega) :\ v|_T \in P_{k+1}(T) \quad \forall T \in \mathfrak{I}_h \right\}, \\ \mathbf{X}_h &= \left\{ \mathbf{v} \in \mathbf{H}_0(\text{curl},\Omega) : \mathbf{v}|_T \in \mathbf{P}_k(T) \quad \forall T \in \mathfrak{I}_h \right\}, \end{aligned} \tag{11}$$

where $P_k(T)$ is the space of polynomials of order $k > 0$ and $\mathbf{P}_k(T) = \left(P_k(T)\right)^3$. Similar to (9), we define the ICST-finite element space as follows

$$\mathbf{U}_h = \left\{ \chi\cdot\nabla\varphi_h :\ \varphi_h \in \mathrm{Y}_h \right\}. \tag{12}$$

Given $\mathbf{A}_0 = \mathbf{u}_0 = 0$, the fully discrete approximation to (10) reads: Find $\mathbf{A}_n \in \mathbf{X}_h$, $\mathbf{u}_n \in \mathbf{U}_h$, $n \geq 1$ such that

$$\begin{aligned} &\int_\Omega \sigma \frac{\delta(\mathbf{A}_n + \mathbf{u}_n)}{\delta t} \cdot (\mathbf{v}_h + \mathbf{w}_h) + \int_\Omega \nu \,\mathrm{curl}\mathbf{A}_n \cdot \mathrm{curl}\mathbf{v}_h \\ &\quad = \int_\Omega \mathbf{J}_n \cdot (\mathbf{v}_h + \mathbf{w}_h) \quad \forall \mathbf{v}_h \in \mathbf{X}_h, \mathbf{w}_h \in \mathbf{U}_h, \end{aligned} \tag{13}$$

where $\mathbf{v}_h, \mathbf{w}_h$ are discrete test functions and

$$\frac{\delta w_n}{\delta t} = \frac{w_n - w_{n-1}}{\tau_n}, \qquad \mathbf{J}_n = \frac{1}{\tau_n}\int_{t_{n-1}}^{t_n} \mathbf{J}_s(t)\mathrm{d}t.$$

Let $\{\mathbf{b}_1, \cdots, \mathbf{b}_{J_1}\}$ and $\{\mathbf{q}_1, \cdots, \mathbf{q}_{J_2}\}$ be the nodal bases of $\mathbf{X}_h$ and $\mathbf{U}_h$ respectively. Then $\mathbf{A}_n, \mathbf{u}_n$ can be represented by the linear combinations of these basis functions:

$$\mathbf{A}_n = \sum_{i=1}^{J_1} A_n^i \mathbf{b}_i, \qquad \mathbf{u}_n = \sum_{i=1}^{J_2} u_n^i \mathbf{q}_i.$$

Now taking $\mathbf{v}_h = \mathbf{b}_j, 1 \leq j \leq J_1$ and $\mathbf{w}_h = \mathbf{q}_j, 1 \leq j \leq J_2$ in (13) respectively, we get an equivalent system of algebraic equations

$$\mathbf{M}(\boldsymbol{Z}_n) \cdot \boldsymbol{Z}_n = \boldsymbol{F}_n, \tag{14}$$

where $\boldsymbol{Z}_n = (A_n^1, \cdots, A_n^{J_1}, u_n^1, \cdots, u_n^{J_2})^t$ and $\mathbf{M}(\boldsymbol{Z}_n)$ is the stiffness matrix defined by

$$\begin{aligned} M_{ij} &= \int_\Omega \frac{\sigma}{\tau_n} \mathbf{b}_i \cdot \mathbf{b}_j + \int_\Omega \nu \mathrm{curl}\mathbf{b}_i \cdot \mathrm{curl}\mathbf{b}_j, \; 1 \leq i, j \leq J_1, \\ M_{i+J_1, j+J_1} &= \int_\Omega \frac{\sigma}{\tau_n} \mathbf{q}_i \cdot \mathbf{q}_j, \qquad 1 \leq i, j \leq J_2, \\ M_{i, j+J_1} &= \mathrm{M}_{j+J_1, i} = \int_\Omega \frac{\sigma}{\tau_n} \mathbf{b}_i \cdot \mathbf{q}_j, 1 \leq i \leq J_1, 1 \leq j \leq J_2. \end{aligned} \tag{15}$$

Clearly $\mathbf{M}(\boldsymbol{Z}_n)$ depends on $\boldsymbol{Z}_n$ through the nonlinear reluctivity. The entries of $\boldsymbol{F}_n$ are defined by

$$\begin{aligned} F_n^i &= \int_\Omega \left(\mathbf{J}_n + \tau_n^{-1}\sigma \mathbf{A}_{n-1}\right) \cdot \mathbf{b}_i, \quad 1 \leq i \leq J_1, \\ F_n^{i+J_1} &= \int_\Omega \left(\mathbf{J}_n + \tau_n^{-1}\sigma \mathbf{A}_{n-1}\right) \cdot \mathbf{q}_i, \quad 1 \leq i \leq J_2. \end{aligned}$$

We are going to solve the nonlinear problem (14) by inexact Newton method (cf. e.g. [19, Section 1.4]):

$$\boldsymbol{Z}_n^{(k+1)} = \boldsymbol{Z}_n^{(k)} + \alpha_k \widetilde{\boldsymbol{E}}, \;\; k \geq 0, \qquad \boldsymbol{Z}_n^{(0)} := \boldsymbol{Z}_{n-1}, \tag{16}$$

where $0 < \alpha_k \leq 1$ is the damping factor and $\widetilde{\boldsymbol{E}}$ is an approximate solution of the system of algebraic equations:

$$\hat{\mathbf{M}} \cdot \boldsymbol{E} = \boldsymbol{R}_{n,k}. \tag{17}$$

In fact, (17) is the error equation of (14) for the approximate solution $\boldsymbol{Z}_n^{(k)}$, and $\boldsymbol{R}_{n,k}$ is the residual vector defined by

$$\boldsymbol{R}_{n,k} := \boldsymbol{F}_n - \mathbf{M}(\boldsymbol{Z}_n^{(k)}) \cdot \boldsymbol{Z}_n^{(k)}.$$

Let $(\mathbf{A}_n^{(k)}, \mathbf{u}_n^{(k)})$ be the approximate solutions of (13) associated with $\boldsymbol{Z}_n^{(k)}$. The matrix $\hat{\mathbf{M}}$ is also computed by (15) and by replacing ν with the differential reluctivity $\hat{\nu}$ valued at $(\mathbf{A}_n^{(k)}, \mathbf{u}_n^{(k)})$. The inexactness of the Newton method means that a damping factor α_k and an approximate solution $\widetilde{\boldsymbol{E}}$ of (17) are used at each step.

Algorithm 1 (Inexact Newton Algorithm)

Given the maximal number of iterations $N_{ina} = 50$ and the initial guess $\boldsymbol{Z}_n^{(0)} = \boldsymbol{Z}_{n-1}$. Set $k = 0$.

While $\left\|\boldsymbol{R}_{n,k}\right\| \geq 10^{-3}\left\|\boldsymbol{F}_n\right\|$ & $k \leq N_{ina}$ do

1. Set $\varepsilon = 1 + \left\|\boldsymbol{R}_{n,k}\right\|$ and $\alpha_k = 1/0.618$.
2. Compute an approximate solution $\widetilde{\boldsymbol{E}}$ of (17) by Algorithm 2.
3. While $\varepsilon \geq \left\|\boldsymbol{R}_{n,k}\right\|$ do
   (3.1) $\alpha_k \leftarrow 0.618\alpha_k$;
   (3.2) $\boldsymbol{Z}_n^{(k+1)} = \boldsymbol{Z}_n^{(k)} + \alpha_k \widetilde{\boldsymbol{E}}$;
   (3.3) $\varepsilon = \left\|\boldsymbol{F}_n - \mathbf{M}(\boldsymbol{Z}_n^{(k+1)}) \cdot \boldsymbol{Z}_n^{(k+1)}\right\|$.
   End While.
4. $k \leftarrow k + 1$.

End While.

To the best of our knowledge, for large numbers of elements, efficient solver is still a difficult issue for discrete Maxwell's equations with nonlinear and anisotropic reluctivity. Accurate solution of (17) requires a long time and makes the Newton method inefficient. To reduce the computational time, we only use an approximate error function $\widetilde{\boldsymbol{E}}$ in (16). The exact solution of (17) is denoted by $\boldsymbol{E} = (E_1, \cdots, E_{J_1+J_2})$ and represents the error functions as follows

$$\mathbf{e}=\sum_{j=1}^{J_1}E_j\mathbf{b}_j,\qquad \boldsymbol{\theta}=\sum_{j=1}^{J_2}E_{j+J_1}\mathbf{q}_j.$$

Then (17) is equivalent to the discrete problem: Find $\mathbf{e}\in\mathbf{X}_h$ and $\boldsymbol{\theta}\in\mathbf{U}_h$ such that

$$\begin{aligned}&\int_\Omega\frac{\sigma}{\tau_n}(\mathbf{e}+\boldsymbol{\theta})\cdot(\mathbf{v}_h+\mathbf{w}_h)+\int_\Omega\hat{\nu}\,\mathrm{curl}\,\mathbf{e}\cdot\mathrm{curl}\,\mathbf{v}_h\\&\quad=r_{n,k}(\mathbf{v}_h,\mathbf{w}_h)\quad\forall\,\mathbf{v}_h\in\mathbf{X}_h,\ \mathbf{w}_h\in\mathbf{U}_h,\end{aligned}\tag{18}$$

where $r_{n,k}$ is the residual functional defined by

$$\begin{aligned}r_{n,k}(\mathbf{v}_h,\mathbf{w}_h)&=\int_\Omega\mathbf{J}_n\cdot(\mathbf{v}_h+\mathbf{w}_h)-\int_\Omega\nu\mathrm{curl}\mathbf{A}_n^{(k)}\cdot\mathrm{curl}\mathbf{v}_h\\&\quad-\int_\Omega\frac{\sigma}{\tau_n}\left(\mathbf{A}_n^{(k)}+\mathbf{u}_n^{(k)}-\mathbf{A}_{n-1}-\mathbf{u}_{n-1}\right)\cdot(\mathbf{v}_h+\mathbf{w}_h).\end{aligned}$$

Now we propose an alternating iteration algorithm to compute an approximate solution $\tilde{\boldsymbol{E}}$ of (17).

Algorithm 2 (Alternating Iteration Algorithm)

Given the maximal number of iterations $N_{aia}=10$ and the initial guess $\boldsymbol{E}_0=0$ and $\mathbf{e}_0=0$. Set $l=0$.

1. While $\left\|\boldsymbol{R}_{n,k}-\hat{\mathbf{M}}\cdot\boldsymbol{E}_l\right\|\ge10^{-2}\left\|\boldsymbol{R}_{n,k}\right\|$ & $l\le N_{aia}$ do

   1.1 Solve the following elliptic problem by 5 iterations of conjugate gradient method preconditioned by the Boomer-AMG (Algebraic Multigrid) method [20]:
   Find $\phi_{l+1}\in\mathrm{Y}_h$ such that

$$\begin{aligned}\int_\Omega\chi\sigma\nabla\phi_{l+1}\cdot\nabla\varphi_h&=\tau_n r_{n,k}(0,\chi\nabla\varphi_h)\\&\quad-\int_\Omega\chi\sigma\mathbf{e}_l\cdot\nabla\varphi_h\quad\forall\varphi_h\in\mathrm{Y}_h.\end{aligned}$$

   1.2 Solve the following Maxwell equation by 10 iterations of preconditioned conjugate gradient (PCG) method with the HX-preconditioner [21]:
   Find $\mathbf{e}_{l+1}\in\mathbf{X}_h$ such that

$$\begin{aligned}&\int_\Omega\sigma\,\mathbf{e}_{l+1}\cdot\mathbf{v}_h+\tau_n\int_\Omega\hat{\nu}\,\mathrm{curl}\,\mathbf{e}_{l+1}\cdot\mathrm{curl}\,\mathbf{v}_h\\&=\tau_n r_{n,k}(\mathbf{v}_h,0)-\int_\Omega\sigma\chi\cdot\nabla\phi_{l+1}\cdot\mathbf{v}_h\quad\forall\mathbf{v}_h\in\mathbf{X}_h.\end{aligned}$$

   1.3 Compute $\boldsymbol{E}_{l+1}$ from $(\mathbf{e}_{l+1},\boldsymbol{\theta}_{l+1})$ and set $l\leftarrow l+1$.

   End While.

2. Set $\tilde{\boldsymbol{E}}=\boldsymbol{E}_l$.

Since Algorithm 2 only computes an approximate solution of (17), to reduce the computational time, we set the maximal number of iterations by $N_{aia}=10$. In each alternating iteration, we only use 5 iterations of PCG method for solving ϕ_{l+1} and 10 iterations of PCG method for solving $\mathbf{e}_{l+1}$. Since the Boomer-AMG method is very efficient in solving second-order elliptic problems, we use less iterations in Step 1.1 than in Step 1.2. In fact, the computational time for Step 1.1 is negligible compared with that for Step 1.2.

V. Numerical Experiments

In this section, we report the numerical experiment based on the TEAM Workshop Problem 21^c-M1 [22]. The conducting region, referred to as a magnetic shield configuration, is the combination of a lamination stack and a magnetic plate whose dimensions are respectively $6\times270\times458$ mm^3 and $10\times360\times520$ mm^3, as shown in Fig. 5. The lamination stack consists of 20 steel sheets and the coating film over each sheet is 4μm thick. The source currents are carried in opposite directions by two coils and are 3000 Ampere/Turn at a frequency of 50Hz, namely,

$$\mathbf{J}_s(\mathbf{x},t)=\hat{\mathbf{J}}_s(\mathbf{x})\cdot\sin(100\pi t),\quad t\ge0.$$

The height of each coil is 217mm and the radiuses of the inner arc and the outer arc at four corners are 10mm and 45mm respectively. The distance between the lamination stack and the coils is 12mm and the vertical distance between the two coils is 24mm.

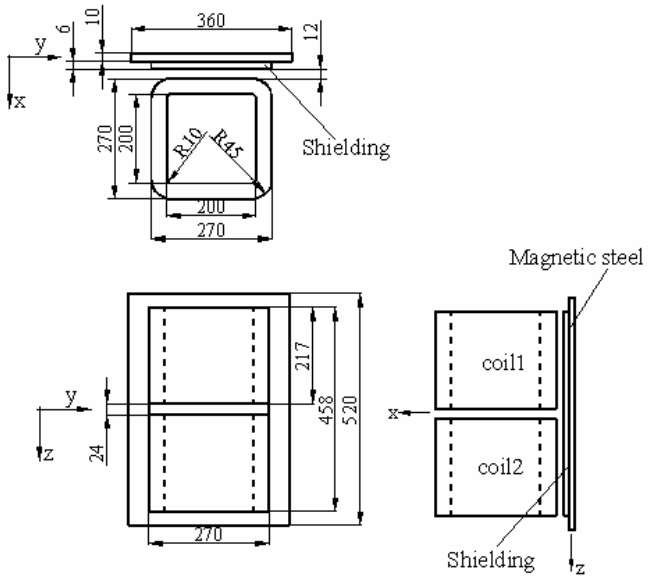

Fig. 5 TEAM Workshop Problem 21^c-M1(all dimensions are in mm).

We use the second-order edge element method of the second family [23] to solve the problem, that is, setting $k=2$ in (11). The implementation is based on the adaptive finite element package "**P**arallel **H**ierarchical **G**rid" (PHG) [24].

The computations are carried out on 512 CPU cores on the cluster LSEC-III, the State Key Laboratory on Scientific and Engineering Computing, Chinese Academy of Sciences.

The domain Ω is meshed into 9.0×10^6 tetrahedra and each lamination is subdivided into three layers in the normal direction to the lamination plane. The number of degrees of freedom on the mesh is 1.26×10^8. The purpose of this experiment is as follows:

1. To validate the new **A**-formulation (10) of the eddy current model by reducing the influence of the numerical error.
2. To demonstrate the approximation of the finite element problem (13) to the continuous problem (10).
3. To examine 3D eddy currents in the laminations.

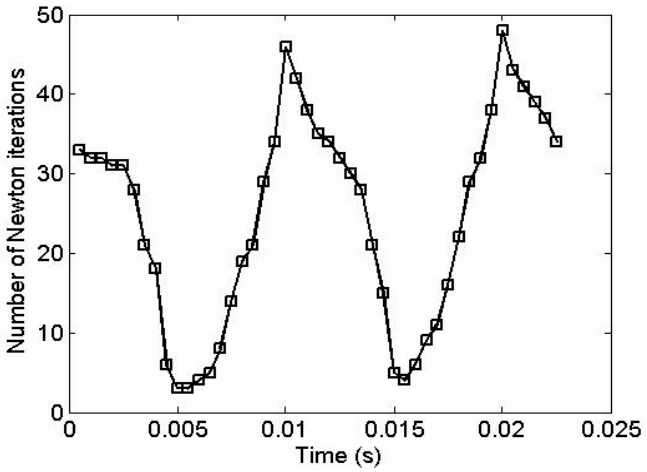

Fig. 6 Number of Newton iterations such that the relative residual is less than 10^{-3}.

The end time is set by the length of two periods of the source current and is given by $t_{end}=0.04\text{s}$. The interval $[0,t_{end}]$ is partitioned uniformly into 80 time steps such that $\tau_n=5\times10^{-4}\text{s}$ for all $n>0$. Unlike isotropic materials, the anisotropic reluctivity influences the number of Newton iterations. The criterion $\left\|\boldsymbol{R}_{n,k}-\hat{\mathbf{M}}\cdot\boldsymbol{E}_l\right\|<10^{-2}\left\|\boldsymbol{R}_{n,k}\right\|$ is not always satisfied in Algorithm 2, and in that case, we use 10 alternating iterations to save the computational time. Fig. 6 shows the number of Newton iterations to attain the criterion $\left\|\boldsymbol{R}_{n,k}\right\|<10^{-3}\left\|\boldsymbol{F}_n\right\|$ at all time steps within the first period. The method converges slowly at $t_n=0.01\text{s}$, 0.02s, 0.03s, and 0.04s.

To validate the new formulation (10), the numerical results are compared with the experimental data measured by the R & D center of Baoding Tianwei Group Co., LTD, China, which can be found in [22]. Figs. 7-8 show the calculated values of the magnetic flux density on a coarse mesh with 187,152 tetrahedra and a fine mesh with 9,000,628 tetrahedra. The numerical values from the coarse mesh have larger errors on a few points, while the numerical values on the fine mesh agree well with the measurement data. TABLE I shows the calculated iron loss on the fine mesh and the numerical value is close to the experimental value. The numerical experiment indicates that the new formulation (10), or the ICST, provides an accurate approximation to the original problem (2), and the discrete problem (13) is a good approximation to (10).

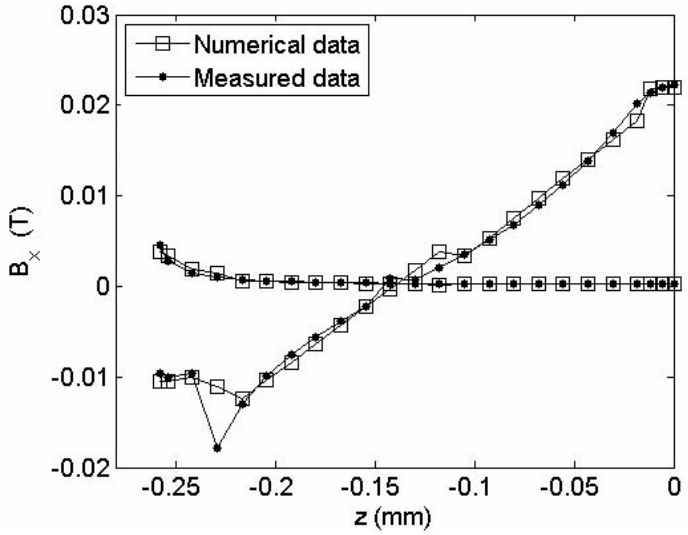

Fig. 7 Magnetic flux density: the numerical data still have large errors at a few points by a mesh with 187,152 elements.

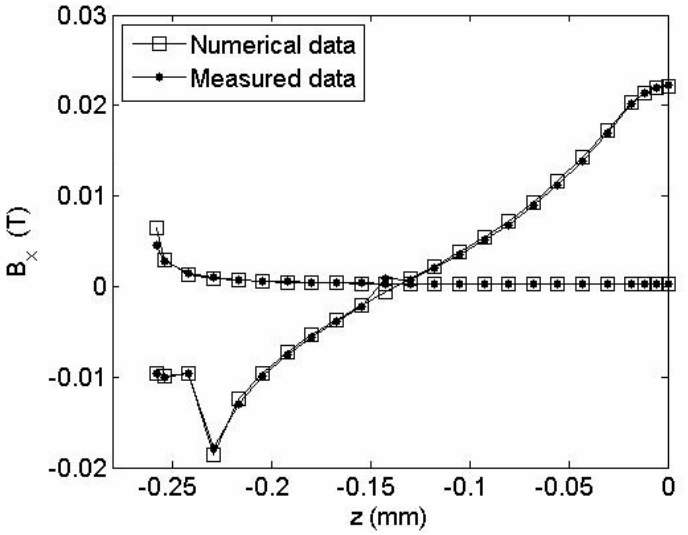

Fig. 8 Magnetic flux density: the numerical data agree well with the measurement data by a mesh with 9,000,628 elements.

TABLE I
IRON LOSS IN THE LAMINATION AND THE MAGNETIC PLATE (W)

Calculated iron loss			Measured iron loss
Loss in the lamination	Loss in the magnetic plate	Total loss	
2.789	0.941	3.73	3.72

Figs. 9-10 show the tangential component of the eddy current density in Ω_1 and Ω_2 respectively, where Ω_i is the lamination whose distance is $d_i=(11.7+0.3i)$ mm from

the coils, $i = 1,2$. The eddy current density in the second sheet is reduced considerably compared with that of the first sheet. Fig. 11 shows the eddy current density on one slice of the magnetic plate which is 2mm away from the lamination stack. It shows a shielded area by the lamination stack.

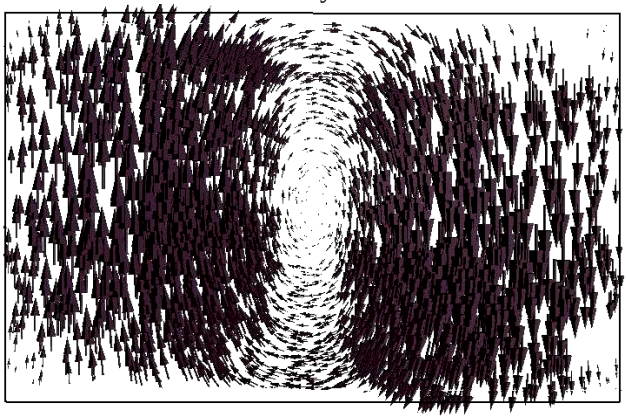

Fig. 9 Eddy current distribution in the first lamination.

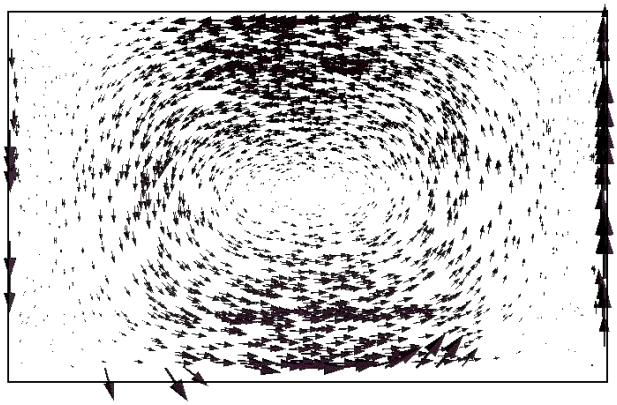

Fig. 10 Eddy current distribution in the second lamination.

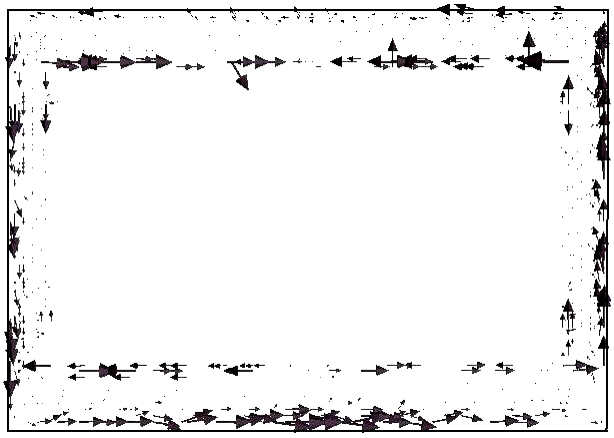

Fig. 11 Eddy current distribution on the slice being 2mm away from the lamination stack.

VI. Conclusion

An inner-constrained separation technique is proposed for computing 3D eddy currents in GO silicon steel laminations. The ICST yields a new **A**-formulation of the eddy current problem and is efficient in simulating 3D eddy currents without meshing coating films. A parallel finite element program is developed to solve the new formulation based on MPI and unstructured tetrahedral meshes.

Acknowledgment

The authors would like to thank Prof. Zhiming Chen, Prof. Linbo Zhang, Dr. Tao Cui of Academy of Mathematics and Systems Science, Chinese Academy of Sciences, for their valuable discussions and suggestions. This work was supported in part by the National Magnetic Confinement Fusion Science Program (Grant No. 2011GB105003), by China NSF under the grants 11031006 and 11171334, and by the Funds for Creative Research Groups of China (Grant No. 11021101).

References

[1] A. De Rochebrune, J. M. Dedulle, and J. C. Sabonnadiere, “A technique of homogenization applied to the modeling of transformers,” *IEEE Trans. Magn.*, vol. 26, no.2, pp.520-523, 1990.

[2] A. J. Bergqvist and S. G. Engdahl, “A homogenization procedure of field quantities in laminated electric steel”, *IEEE Trans. Magn*., vol. 37, no. 5, pp. 3329–3331, 2001.

[3] I. Sebestyen, S. Gyimothy, J. Pavo, and O. Biro, “Calculation of losses in laminated ferromagnetic materials”, *IEEE Trans. Magn.*, vol. 40, no.2, pp.924-927, 2004.

[4] H. Kaimori, A. Kameari, and K. Fujiwara, “FEM computation of magnetic field and iron loss using homogenization method”, *IEEE Trans. Magn.*, vol.43, no.2, pp.1405-1408, 2007.

[5] A. Bermúdez, D. Gómez, and P. Salgado, “Eddy-current losses in laminated cores and the computation of an equivalent conductivity”, *IEEE Trans. Magn.*, vol. 44, no. 12, pp. 4730–4738, 2008.

[6] O. Bottauscio, V. Chiadopiat, M. Chiampi, M. Codegone, and A. Manzin, “Nonlinear homogenization technique for saturable soft magnetic composites,” *IEEE Trans. Magn.*, vol. 44, no. 11, pp. 2955–2958, 2008.

[7] O. Bottauscio, M. Chiampi, and A. Manzin, “Homogenized magnetic properties of heterogeneous anisotropic structures including nonlinear media”, *IEEE Trans. Magn.*, vol. 45, no. 3, pp. 1276–1279, Mar. 2009.

[8] J. Gyselinck and P. Dular, “A time-domain homogenization technique for laminated iron cores in 3D finite element models”, *IEEE Trans. Magn.*, vol. 40, no. 3, pp. 1424–1427, May 2004.

[9] J. Gyselinck, R. V. Sabariego, and P. Dular, “A nonlinear time-domain homogenization technique for laminated iron cores in three-dimensional finite-element models,” *IEEE Trans. Magn.*, vol. 42, no. 4, pp. 763–766, 2006.

[10] N. Hihat, E. Napieralska-Juszczak, J. P. Lecointe, J. K. Sykulski, and K. Komeza, “Equivalent permeability of step-lap joints of transformer cores: computational and experimental considerations”, *IEEE Trans. Magn.*, vol. 47, no. 1, pp. 244–251, 2011.

[11] Z. Cheng, N. Takahashi, B. Forghani, G. Gilbert, J. Zhang, L. Liu, Y. Fan, X. Zhang, Y.Du, J. Wang, and C. Jiao, “Analysis and measurements of iron loss and flux inside silicon steel laminations”, *IEEE Trans. Magn.*, vol. 45, no. 3, pp. 1222–1225, 2009.

[12] Y. Du, Z. Cheng, Z. Zhao, Y. Fan, L. Liu, J. Zhang, and J. Wang, “Magnetic flux and iron loss modeling at laminated core joints in power transformers”, *IEEE Trans. Appl. Supperconductivity*, vol. 20, no. 3, pp. 1878-1882, 2010.

[13] E. Dlala, A. Belahcen, J. Pippuri, and A. Arkkio, “Interdependence of hysteresis and eddy-current losses in laminated magnetic cores of electrical machines”, *IEEE Trans. Magn.*, vol. 46, no. 2, pp. 244–251, 2010.

[14] Z. Cheng, N. Takahashi, S. Yang, T. Asano, Q. Hu, S. Gao, X. Ren, H. Yang, L. Liu, and L. Gou, “Loss spectrum and electromagnetic behavior of Problem 21 family”, *IEEE Trans. Magn.*, vol. 42, no. 4, pp. 1467–1470, 2006.

[15] G. Grandi, M. K. Kazimierczuk, A. Massarini, U. Reggiani, and G. Sancineto, “Model of laminated iron-core inductors for high frequencies”, *IEEE Trans. Magn.*, vol. 46, no. 2, pp. 279–286, 2010.

[16] P. Rovolis, A. Kladas, and J. Tegopoulos, “Numerical and experimental analysis of iron core losses under various frequencies,” *IEEE Trans. Magn.*, vol. 45, no. 3, pp. 1206–1209, 2009.

[17] C. Patsios, E. Tsampouris, M. Beniakar, P. Rovolis, and A. G. Kladas, “Dynamic finite element hysteresis model for iron loss calculation in non-oriented grain iron laminations under PWM excitation”, *IEEE Trans. Magn.*, vol. 40, no.2, pp.924-927, 2004.

[18] M. Clemens, J. Lang, D. Teleaga, and G. Wimmer, “Adaptivity in space and time for magnetoquasistatics”, *J. Comp. Math.*, vol. 27, no.5, pp. 642-656, 2009.

[19] P. Deuflhard, “Newton Methods for Nonlinear Problems: Affine Invariance and Adaptive Algorithms”, Springer-Verlag, Berlin, Heidelberg, 2004.

[20] V. E. Henson and U. M. Yang, “BoomerAMG: a parallel algebraic multigrid solver and preconditioner”, Appl. Num. Math., vol. 41, issue 1, pp. 155–177, 2002.

[21] R. Hiptmair and J. Xu, “Auxiliary space preconditioning for edge elements”, *IEEE Trans. on Magnetics*, vol. 44, no.6, pp.938-941, 2008.

[22] Z. Cheng, N. Takahashi, and B. Forghani, “TEAM Problem 21 Family (V.2009)”, approved by the International Compumag Society at Compumag 2009, http://www.compumag.org/jsite/team .

[23] J. C. Nédélec, “A new family of mixed finite elements in R^3”, *Numer. Math.*, vol. 50, no. 1, pp. 57-81, 1986.

[24] L. Zhang, “A Parallel algorithm for adaptive local refinement of tetrahedral meshes using bisection”, Numer. Math.: Theor. Method Appl., 2 (2009) 65–89. http://lsec.cc.ac.cn/phg/ .